4

Void Growth in Plastic Solids

A. Needleman, V. Tvergaard and J.W. Hutchinson

ABSTRACT An overview is given of the continuum mechanics of void growth pertaining to room temperature ductile fracture processes. Analyses of the growth of isolated voids and of void interaction effects are reviewed. A framework for phenomenological constitutive relations for porous plastic solids is discussed. Calculations of localization and failure in porous plastic solids are reviewed that illustrate the progressive development of ductile failure. Additional considerations, including the effect of the constraint provided by contact between the growing void and the void-nucleating particle, cavitation, and the effect of non-uniform porosity distributions are briefly noted.

4.1 Introduction

The role played by void nucleation, growth and coalescence in ductile fracture was identified in the 1940's, Tipper (1949). However, it was not until the 1960's that the phenomenology of this process was well documented, Rogers (1960), Puttick (1960), Beachem (1963), and Gurland and Plateau (1963). In structural metals deformed at room temperature, the voids generally nucleate by decohesion of second phase particles or by particle fracture, and grow by plastic deformation of the surrounding matrix. Void coalescence occurs either by necking down of the matrix material between adjacent voids or by localized shearing between well separated voids.

McClintock's (1968) analysis of the expansion of a long cylindrical hole in an ideally plastic solid marks the beginning of a now extensive literature on the micromechanics of ductile fracture. More broadly, this paper showed that a precise mechanics analysis of a carefully chosen continuum model could serve to quantify complex microstructural behavior. Micromechanics analyses of void nucleation and coalescence, as well as of void growth, have now been carried out. Such analyses have served as the basis for phenomenological constitutive relations for porous plastic solids, which in turn have been used to predict macroscopic ductile fracture behavior. An overview of these developments is given by Tvergaard (1990). Another overview of void growth studies is given in Gilormini, Licht and Suquet (1988).

Our focus in this paper is on issues in the mechanics of void growth relevant to room temperature ductile fracture processes. We begin by reviewing analyses of the growth of an isolated void. A key point in this regard concerns the hydrostatic stress dependence of the void growth rate. The phenomenological framework for constitutive relations for porous plastic solids introduced by Gurson (1975) is outlined, since there has been considerable interplay between analyses based on this constitutive relation and the development of more accurate void growth models.

4.2 Growth of an Isolated Void

Predicting ductile fracture behavior requires knowing the relation between the growth of a void and the imposed stress and strain histories. Of particular importance is the dependence of the rate of void growth on the remote stress triaxiality, which is revealed by tension tests on notched tensile bars, Hancock and Mackenzie (1976), Hancock and Brown (1983). Although the maximum strain occurs at the root of the notch, for certain combinations of notch acuity and stress state (plane strain or axisymmetric), ductile failure initiates inside the specimen where the triaxiality of the stress state is greater than near the surface.

To investigate the stress state dependence of the void growth rate, McClintock (1968) considered a long cylindrical void in an ideally plastic solid, extending in the direction of its axis, as shown in Fig. 4.1. The cylindrical void has current radius b and the aim is to determine the dependence of the void growth rate $\dot{b}/b$ on the imposed axial strain rate $\dot{\epsilon}$ and the transverse stress σ_∞. McClintock's (1968) analysis is summarized here.

Generalized plane strain and cylindrical symmetry are assumed, so that with polar coordinates (r, θ, z), all field quantities are functions solely of r. Equilibrium in the current configuration is written as

$$\frac{d\sigma_r}{dr} + \frac{\sigma_r - \sigma_\theta}{r} = 0 \tag{4.1}$$

The radial displacement is denoted by $u(r)$ and is the only non-vanishing in-plane displacement. With a superposed dot denoting the time derivative, the strain rate-displacement rate relations are

$$\dot{\epsilon}_r = \frac{d\dot{u}}{dr} \qquad \dot{\epsilon}_\theta = \frac{\dot{u}}{r} \tag{4.2}$$

and incompressibility implies

$$\dot{\epsilon}_r + \dot{\epsilon}_\theta + \dot{\epsilon} = 0 \tag{4.3}$$

The flow rule for a Mises solid requires

$$\dot{\epsilon}_r = \frac{3}{2}(\sigma_r - \sigma)\frac{\dot{\bar{\epsilon}}}{Y} \qquad \dot{\epsilon}_\theta = \frac{3}{2}(\sigma_\theta - \sigma)\frac{\dot{\bar{\epsilon}}}{Y} \tag{4.4}$$

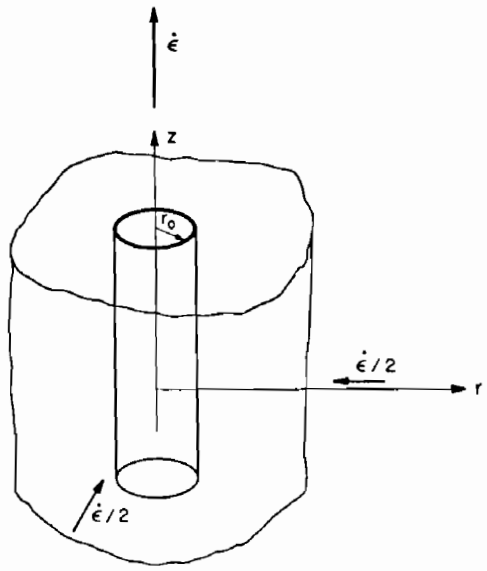

FIGURE 4.1. Long cylindrical void extended along its axis.

where Y is the tensile flow strength and

$$\sigma = \frac{1}{3}(\sigma_r + \sigma_\theta + \sigma_z) \qquad \dot{\bar{\epsilon}} = \sqrt{\frac{2}{3}(\dot{\epsilon}_r^2 + \dot{\epsilon}_\theta^2 + \dot{\epsilon}^2)} \tag{4.5}$$

Here, σ is the mean stress and $\dot{\bar{\epsilon}}$ is the Mises equivalent strain rate.

The boundary conditions are that the radial stress vanishes on the surface of the void and that it takes on its remote value as $r \to \infty$.

$$\sigma_r(b) = 0 \qquad \sigma_r(\infty) = \sigma_\infty \tag{4.6}$$

Solving the flow rule Eq. 4.4 for $(\sigma_r - \sigma_\theta)$ gives,

$$\frac{\sigma_r - \sigma_\theta}{r} = \frac{2Y}{3r}\frac{\dot{\epsilon}_\theta - \dot{\epsilon}_r}{\dot{\bar{\epsilon}}} \tag{4.7}$$

Using Eq. 4.7 in the equilibrium equation and integrating we obtain,

$$\frac{\sigma_\infty}{Y} = \frac{2}{3}\int_b^\infty \left[\frac{\dot{\epsilon}_\theta - \dot{\epsilon}_r}{\dot{\bar{\epsilon}}}\right]\frac{dr}{r} \tag{4.8}$$

The incompressibility condition Eq. 4.3 gives the velocity field $\dot{u}(r)$ in terms of the imposed strain rate $\dot{\epsilon}$ and the void expansion rate $\dot{b}/b$ as,

$$\dot{u} = b^2\left[\frac{\dot{b}}{b} + \frac{\dot{\epsilon}}{2}\right]\frac{1}{r} - \frac{\dot{\epsilon}}{2}r \tag{4.9}$$

so that

$$\dot{\epsilon}_r = -\frac{b^2}{r^2}\left[\frac{\dot{b}}{b} + \frac{\dot{\epsilon}}{2}\right] - \frac{\dot{\epsilon}}{2}$$

$$\dot{\epsilon}_\theta = \frac{b^2}{r^2}\left[\frac{\dot{b}}{b} + \frac{\dot{\epsilon}}{2}\right] - \frac{\dot{\epsilon}}{2}$$

$$\dot{\bar{\epsilon}}^2 = \frac{4}{3}\left[\frac{\dot{b}}{b} + \frac{\dot{\epsilon}}{2}\right]^2 \frac{1}{r^4} + \dot{\epsilon}^2 \tag{4.10}$$

Using these expressions in Eq. 4.8, with the substitutions

$$x = \alpha\frac{b^2}{r^2} \qquad \alpha = \frac{2}{\sqrt{3}}\left[\frac{\dot{b}}{\dot{\epsilon}b} + \frac{1}{2}\right] \tag{4.11}$$

gives

$$\frac{\sigma_\infty}{\sqrt{3}Y} = \int_0^\alpha \frac{dx}{\sqrt{1+x^2}} \tag{4.12}$$

Integrating Eq. 4.12 and rearranging terms gives the dependence of the relative void growth rate, $\dot{b}/\dot{\epsilon}b$, on the transverse stress σ_∞,

$$\frac{\dot{b}}{\dot{\epsilon}b} = \frac{\sqrt{3}}{2}\sinh\left[\frac{\sigma_\infty}{\sqrt{3}Y}\right] - \frac{1}{2} \tag{4.13}$$

McClintock's (1968) exact solution exhibits an exponential increase in the void growth rate with positive transverse stress. This can be contrasted with the linear increase that is predicted for a linear viscous material, Berg (1962). For a spherical void, subject to a general remote stress state, the problem is no longer one dimensional and exact solutions are not available. Rice and Tracey (1969) used a Rayleigh-Ritz method to obtain approximate solutions for the growth of an isolated spherical void surrounded by an ideally plastic matrix, as sketched in Fig. 4.2. At high triaxiality, i.e. for large values of the ratio of remote mean stress, σ_h^∞, to matrix flow strength, Y, their numerical results were well-approximated by

$$\frac{\dot{R}_0}{\dot{\epsilon}R_0} \approx 0.283\exp\left[\frac{3\sigma_h^\infty}{2Y}\right] \approx 0.566\sinh\left[\frac{3\sigma_h^\infty}{2Y}\right] \tag{4.14}$$

Furthermore, Rice and Tracey (1969), found that Eq. 4.14 was a very good approximation even at low triaxialities.

Similar explicit expressions showing the effect of material strain hardening on void growth rates have not yet been obtained for rate independent plastic solids. However, the assumption of non-linear viscous, rather than rate independent strain hardening, material behavior facilitates the analysis. Within this context, Budiansky, Hutchinson and Slutsky (1982) have obtained a high triaxiality approximation for the growth rate of an initially

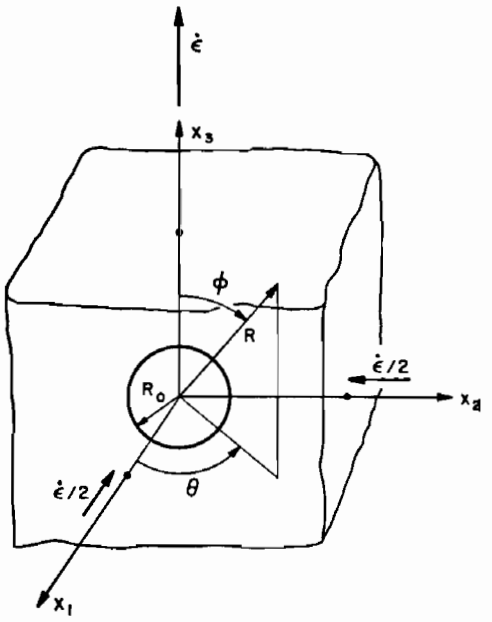

FIGURE 4.2. Spherical void in a remote simple tension strain rate field.

spherical void in a power law viscous solid, i.e. one for which the uniaxial response is $\dot{\epsilon} \propto \sigma^n$, as

$$\frac{\dot{R}_0}{\dot{\epsilon} R_0} = \frac{1}{2}\left[\frac{3\sigma_h^\infty}{2n\sigma_e^\infty} + \frac{(n-1)(n+0.4319)}{n^2}\right]^n \tag{4.15}$$

In the limit $n \to \infty$, the response of the power law viscous solid approaches that of a rigid-ideally plastic Mises solid. In this limit, Eq. 4.15 reduces to Eq. 4.14.

This consistent picture persisted until 1989. In the course of a study of cavitation instabilities in elastic-plastic solids Huang, Hutchinson and Tvergaard (1991) obtained finite element results for the growth of an isolated spherical void in ideally plastic solid that were about 50% higher than expected based on the Rice-Tracey formula Eq. 4.14. This discrepancy was investigated further by Huang (1989) who carried out a Rayleigh-Ritz analysis using a much larger number of terms than Rice and Tracey (1969) and Budiansky et al. (1982). Huang (1989) found that a surprisingly large number of terms were needed to obtain a converged value for the void growth rate and that when a sufficient number of terms were included in the analysis, the Rayleigh-Ritz results were consistent with finite element solutions in Huang et al. (1991). Huang's (1989) high triaxiality approximation is

$$\frac{\dot{R}_0}{\dot{\epsilon} R_0} \approx 0.427 \exp\left[\frac{3\sigma_h^\infty}{2Y}\right] \tag{4.16}$$

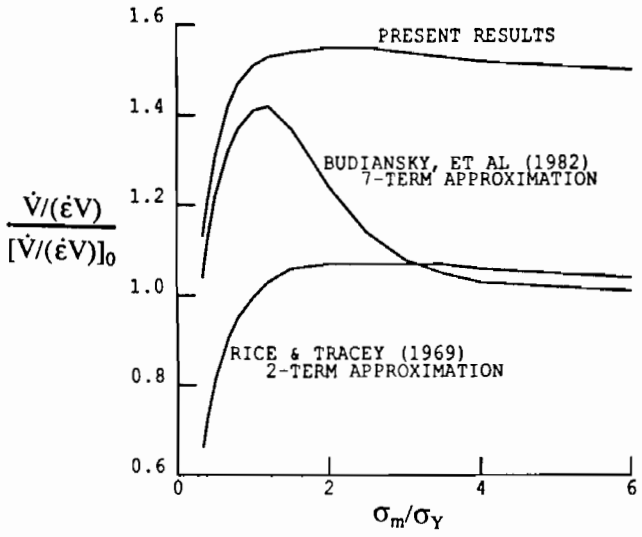

FIGURE 4.3. Dilation rate in a rigid-perfectly plastic solid as computed at various levels of approximation. The volumetric growth rate is normalized by that obtained from Eq. 4.14 using $(\dot{V}/\dot{\epsilon}_0 V)_0 = 3\dot{R}_0/\dot{\epsilon}_0 R_0$ (from Huang, 1989).

This correction is important because the expression for the growth rate of an isolated spherical void is used explicitly in direct predictions of ductility, e.g. Marini, Mudry and Pineau (1985), or implicitly in phenomenological constitutive relations for porous plastic solids, e.g. Gurson (1975). Figure 4.3 compares the void growth rates for a perfectly plastic solid predicted by the analyses of Rice and Tracey (1969), Budiansky et al. (1982) and Huang (1989).

4.3 Constitutive Relations for Porous Plastic Solids

In general, the flow potential for a porous plastic solid can be written in the form

$$\Phi(\boldsymbol{\sigma}, \mathcal{H}, \mathcal{F}) = 0 \tag{4.17}$$

where $\boldsymbol{\sigma}$ denotes the Cauchy stress tensor, $\mathcal{H}$ are a set of properties characterizing the plastic flow of the matrix and $\mathcal{F}$ are a set of properties characterizing the porosity. In practice, only special cases of the form

$$\Phi(\sigma_e, \sigma_h, \bar{\sigma}, f) = 0 \tag{4.18}$$

and satisfying

$$\Phi = \frac{\sigma_e^2}{\bar{\sigma}^2} - 1 = 0 \qquad \text{when } f = 0 \tag{4.19}$$

have been considered, e.g. by Gurson (1975), Shima and Oyane (1976), Guennouni and Francois (1987). Here, the hydrostatic stress, σ_h, and the Mises effective stress, σ_e, are given by

$$\sigma_h = \frac{1}{3}\sigma_{kk} \quad \sigma_e = \sqrt{\frac{3}{2}\sigma'_{ij}\sigma'_{ij}} \tag{4.20}$$

In Eq. 4.20 and subsequently, Cartesian tensor notation is employed.

The most widely used porous plastic constitutive relation for analyzing ductile fracture phenomena is that due to Gurson (1975), which is based on averaging techniques similar to those used by Bishop and Hill (1951). Gurson (1975) approximated a solid with a volume fraction f of voids by a homogeneous spherical body with a spherical cavity. An approximate rigid-plastic limit analysis of this situation was used to develop the yield condition

$$\Phi = \frac{\sigma_e^2}{\bar{\sigma}^2} + 2f\cosh\left(\frac{3\sigma_h}{2\bar{\sigma}}\right) - 1 - f^2 = 0 \tag{4.21}$$

where $\bar{\sigma}$ is an internal variable representing the average strength of the matrix material. Figure 4.4 sketches the shape of the yield surface at various levels of porosity. When $f = 1$, the yield surface shrinks to a point and the material's stress carrying capacity vanishes. The yield function Eq. 4.21 has the following characteristics; (i) it reduces to that for a Mises solid when $f = 0$, (ii) the dependence on void volume fraction is linear when $\sigma_h = 0$, (iii) the dependence on stress triaxiality, $\sigma_h/\bar{\sigma}$, is exponential.

The plastic part of the rate of deformation tensor, D^p_{ij}, is given by the flow rule

$$D^p_{ij} = \dot{\Lambda}\frac{\partial\Phi}{\partial\sigma_{ij}} \qquad D_{ij} = \frac{1}{2}\left(\frac{\partial\dot{u}_i}{\partial x_j} + \frac{\partial\dot{u}_j}{\partial x_i}\right) \tag{4.22}$$

where u_i are the Cartesian components of the displacement vector and a superposed dot denotes partial differentiation with respect to time.

Evolution equations need to be specified for the internal variables f and $\bar{\sigma}$. In general, the evolution of the void volume fraction results from both nucleation of new voids and from growth of existing voids, but void nucleation is not considered here. The growth rate of existing voids is determined by requiring the matrix material to be plastically incompressible. With V_v denoting the void volume and V_m the matrix volume, $f = V_v/(V_v+V_m)$. Differentiating with respect to time and using $\dot{V}_m = 0$, so that $D^p_{kk} = \dot{V}_v/(V_v+V_m)$,

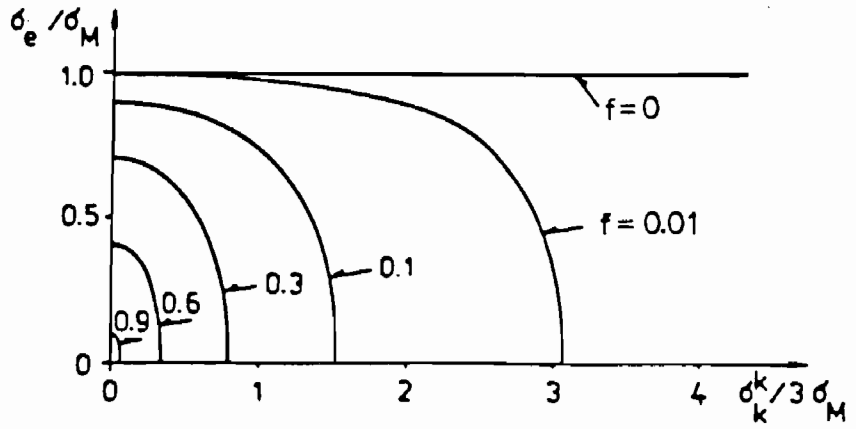

FIGURE 4.4. Yield surface dependence on the hydrostatic tension for various values of porosity, f, in Eq. 4.21.

gives,

$$\dot{f} = (1 - f)D^p_{kk} \tag{4.23}$$

The plastic work rate for the porous solid is set equal to the matrix plastic work rate. Accordingly,

$$\sigma_{ij}D^p_{ij} = (1 - f)\,\bar{\sigma}\,\dot{\bar{\epsilon}} \tag{4.24}$$

From Eq. 4.24, the plastic flow proportionality factor, $\dot{\Lambda}$, in the flow rule Eq. 4.22 is determined to be,

$$\dot{\Lambda} = \frac{(1 - f)\,\bar{\sigma}\dot{\bar{\epsilon}}}{\sigma_{kl}\dfrac{\partial \Phi}{\partial \sigma_{kl}}} \tag{4.25}$$

Here, $\dot{\bar{\epsilon}}$ is the matrix Mises equivalent strain rate, which is determined from the matrix strain hardening relation

$$\dot{\bar{\epsilon}} = \left(\frac{1}{E_t} - \frac{1}{E}\right)\dot{\bar{\sigma}} = \frac{1}{\bar{h}}\dot{\bar{\sigma}} \tag{4.26}$$

where E and E_t are, respectively, the Young's modulus and the tangent modulus, the slope of the uniaxial true stress-logarithmic strain curve, of the matrix material.

Substituting Eq. 4.26 in Eq. 4.24 and rearranging gives the evolution equation for $\dot{\bar{\sigma}}$ as

$$\dot{\bar{\sigma}} = \frac{\bar{h}\sigma_{ij}D^p_{ij}}{(1 - f)\,\bar{\sigma}} \tag{4.27}$$

The flow rule for the porous aggregate is obtained from the consistency condition that $\Phi(\sigma_{ij}, \bar{\sigma}, f) = 0$ for continued plastic loading. Hence,

$$\dot{\Phi} = \frac{\partial \Phi}{\partial \sigma_{ij}} \dot{\sigma}_{ij} + \frac{\partial \Phi}{\partial \bar{\sigma}} \dot{\bar{\sigma}} + \frac{\partial \Phi}{\partial f} \dot{f} = 0 \tag{4.28}$$

Substituting (4.22), (4.23), (4.25) and (4.27) in (4.28) gives

$$D^p_{ij} = \frac{1}{h} \left(\frac{\partial \Phi}{\partial \sigma_{kl}} \dot{\sigma}_{kl} \right) \frac{\partial \Phi}{\partial \sigma_{ij}} = \frac{1}{h} \left(\frac{\partial \Phi}{\partial \sigma_{kl}} \hat{\sigma}_{kl} \right) \frac{\partial \Phi}{\partial \sigma_{ij}} \tag{4.29}$$

where $\hat{\sigma}_{kl}$ is the Jaumann derivative of Cauchy stress and

$$h = -\left[(1-f) \frac{\partial \Phi}{\partial f} \frac{\partial \Phi}{\partial \sigma_{kk}} + \frac{\bar{h}}{(1-f)\bar{\sigma}} \frac{\partial \Phi}{\partial \bar{\sigma}} \left(\sigma_{kl} \frac{\partial \Phi}{\partial \sigma_{kl}} \right) \right] \tag{4.30}$$

The expression (4.29) pertains to plastic loading, which is when $(\sigma_{kl} \partial \Phi / \partial \sigma_{kl})/h > 0$. Otherwise, $D^p_{ij} = 0$.

For an elastic-plastic solid, we write

$$D_{ij} = D^e_{ij} + D^p_{ij} \tag{4.31}$$

In circumstances where the elastic strains remain small, although the plastic strains may be large, it is convenient to use a hypoelastic approximation for D^e_{ij} that has the form

$$\hat{\sigma}_{ij} = \frac{E}{1+\nu} \left[D^e_{ij} + \frac{\nu}{(1-2\nu)} D^e_{kk} \delta_{ij} \right] = L^e_{ijkl} D^e_{kl} \tag{4.32}$$

where E is Young's modulus, ν is Poisson's ratio and δ_{ij} is Kronecker's delta.

Combining (4.29), (4.31) and (4.32) gives, for plastic loading,

$$\hat{\sigma}_{ij} = \left[L^e_{ijkl} - \frac{P_{ij} P_{kl}}{h + P_{mn} L^e_{mnpq} P_{pq}} \right] D_{kl} \tag{4.33}$$

where

$$P_{ij} = L^e_{ijkl} \frac{\partial \Phi}{\partial \sigma_{kl}} \tag{4.34}$$

In ductile fracture processes, the porosity is typically very small until just prior to fracture, when the material's stress carrying capacity is reducing rapidly. In such circumstances, the effects of porosity on plastic response dominate the effects on elastic response, so that the dependence of E and ν on porosity can be neglected. However, when appropriate, the dependence of the elastic properties on porosity can be accounted for, see Fleck et al. (1991), as in continuum damage mechanics, Lemaitre (1985).

Figure 4.5 shows curves of σ_e and of f versus overall effective strain for a material element subject to uniaxial tension with a superposed hydrostatic stress. The stress ratio $T = \sigma_h/\sigma_e$ is constant throughout the deformation history. The initial porosity is $f_0 = 0.002$ and the matrix is assumed ideally plastic. The elastic properties of the matrix are given by $\sigma_0/E = 0.004$ and $\nu = 0.3$. The large effect of stress triaxiality on void growth and aggregate stress-strain response is evident in this figure.

It is worth separating the general features of the framework introduced by Gurson (1975) from the specifics of the particular flow rule. The general features are (i) the one parameter characterization of porosity; (ii) the use of matrix incompressibility to obtain the evolution equation for the void volume fraction and (iii) the use of the equivalence of aggregate and matrix rate of plastic work to relate aggregate hardening to matrix plastic response. The particulars are the specific form of the yield function (Eq. 4.21) and the characterization of the matrix material as a rate independent isotropically hardening solid in Eq. 4.26.

4.4 Localization in Porous Solids

During the deformation of ductile solids it is frequently observed that a rather smoothly varying deformation pattern grows into a pattern involving highly localized deformations in the form of shear bands. Then, final shear fracture often occurs at an overall strain, which is only slightly larger than that at the onset of localization, and failure tends to occur by a void-sheet mechanism, where small voids coalesce inside the shear band as the localized strains grow large. When voids are represented in terms of a ductile porous material model, such as the Gurson model, the onset of flow localization can be studied by a simple model analysis, and such analyses predict that the critical strain for localization is significantly reduced by the presence of voids in the elastic-plastic material (Rice, 1977; Yamamoto, 1978).

For rate independent solids, the onset of localization can be formulated as a bifurcation problem within the framework of a material instability analysis, Hadamard (1903), Hill (1962), Mandel (1966), Rice (1977), with the mode of localization corresponding to a shear band. All-around displacement conditions are imposed so as to rule out geometric instabilities. An element of a solid is considered subject to displacement boundary conditions that in a homogeneous (and homogeneously deformed) solid would give rise to a uniform deformation gradient field. Conditions are sought under which bifurcation into a localized band mode can occur. Within this framework the onset of localization coincides with the loss of ellipticity of the equations governing rate equilibrium.

Current values of field quantities and material properties inside and outside the band are presumed identical so that one possible solution for the

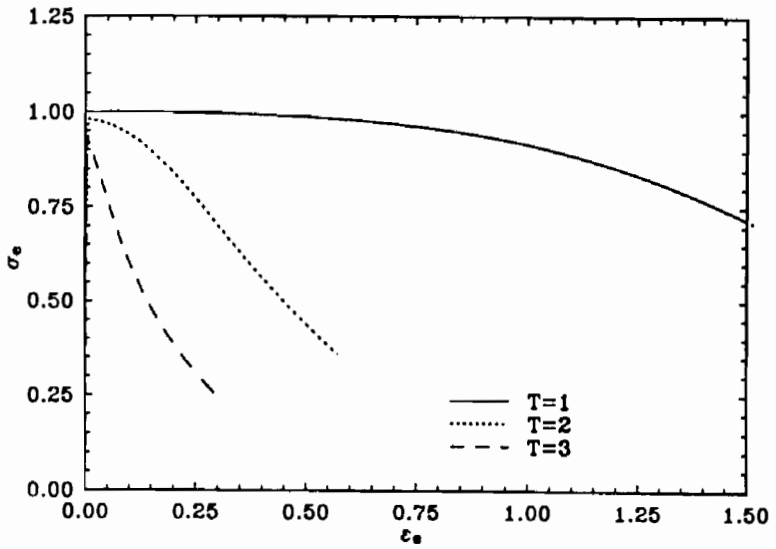

(a)

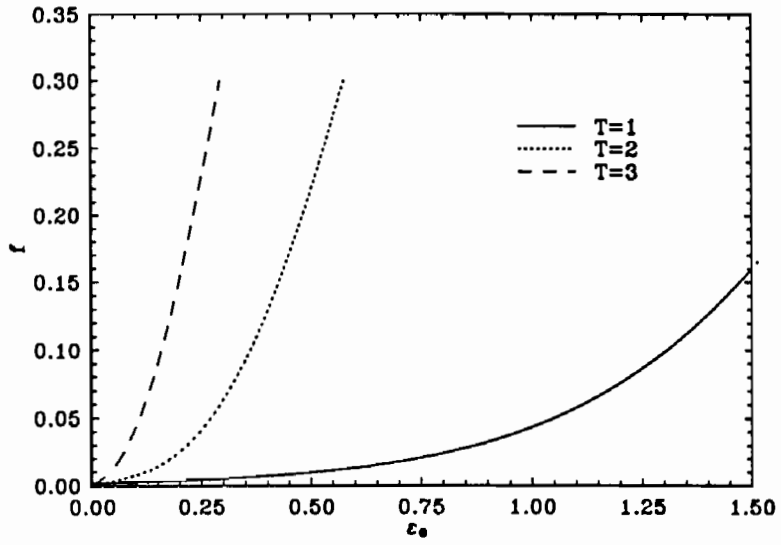

(b)

FIGURE 4.5. (a) Aggregate effective stress, σ_e, versus effective strain, ϵ_e, and (b) void volume fraction, f versus effective strain, ϵ_e, for a material element subject to uniaxial tension with a superposed hydrostatic tension, σ_h, with $T = \sigma_h/\sigma_e$. The original Gurson yield function relation, Eq. 4.21, is used, the matrix is ideally plastic and $f_0 = 0.002$.

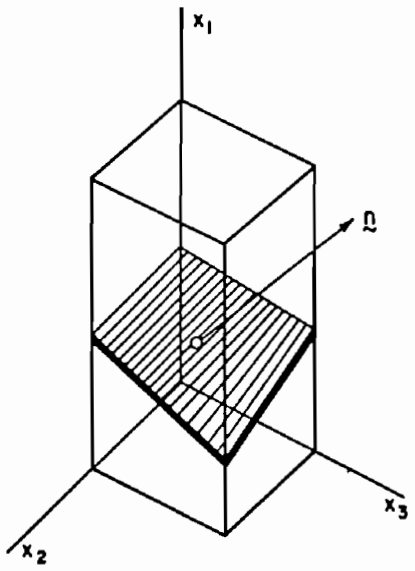

FIGURE 4.6. Body with an incipient band or plane of imperfection.

incremental quantities corresponds to the homogeneous one. At the considered stage of the deformation history, suppose that, as sketched in Fig. 4.6, within a thin planar band of orientation $\mathbf{n}$ in the reference configuration incremental field quantities are permitted to take on values differing from the uniform values outside the band. The band is presumed sufficiently narrow to be regarded as homogeneously deformed.

Two requirements must be satisfied across the band interface. First, compatibility requires continuity of the displacement rate. With the reference and current configurations taken to coincide, this implies,

$$\frac{\partial \dot{u}_i^b}{\partial x_j} = \frac{\partial \dot{u}_i^o}{\partial x_j} + \dot{c}_i n_j \tag{4.35}$$

Next, incremental equilibrium requires

$$n_j \dot{\sigma}_{ji}^b = n_j \dot{\sigma}_{ji}^o \tag{4.36}$$

The material stress rate in Eq. 4.36 is related to the Jaumann stress rate by

$$\hat{\sigma}_{ij} = \dot{\sigma}_{ij} + \sigma_{ik}\Omega_{kj} - \Omega_{ik}\sigma_{kj} \qquad \Omega_{ij} = \frac{1}{2}\left(\frac{\partial \dot{u}_i}{\partial x_j} - \frac{\partial \dot{u}_j}{\partial x_i}\right) \tag{4.37}$$

Substituting (4.35), (4.33) and (4.37) into (4.36) results in three homogeneous algebraic equations for the three unknowns $\dot{c}_i$. Setting the determinant of coefficients equal to zero gives the condition for the onset of a

localization bifurcation. The onset of localization depends on stress state as well as on material properties.

With attention restricted to circumstances where $|\boldsymbol{\sigma}|/E$, f and $f\exp(3\sigma_h/2\bar{\sigma})$ are small, Needleman and Rice (1978) solved for the value of the matrix hardening rate at bifurcation. For an initially porous solid, with no nucleation, under plane strain conditions they obtain

$$\left(\frac{\bar{h}}{\bar{\sigma}}\right)_c = \frac{3}{2} f \cosh\left(\frac{3\sigma_h}{2\bar{\sigma}}\right) \sinh\left(\frac{3\sigma_h}{2\bar{\sigma}}\right) \tag{4.38}$$

while for axisymmetric straining

$$\left(\frac{\bar{h}}{\bar{\sigma}}\right)_c = -\frac{E}{4\bar{\sigma}} + \frac{3}{2} f \cosh\left(\frac{3\sigma_h}{2\bar{\sigma}}\right) \sinh\left(\frac{3\sigma_h}{2\bar{\sigma}}\right) \tag{4.39}$$

The matrix hardening rate, $\bar{h}$, varies during the deformation history. Typically, $\bar{h}$, has some positive value at initial yield and then decreases, so that larger values of $\bar{h}$ correspond to earlier stages of the deformation history. For a fully dense solid, $f \equiv 0$, the localization results for an isotropically hardening Mises solid are recovered; an ideally plastic state, $\bar{h}_c = 0$, is needed for localization under plane strain conditions and a strongly negative hardening rate is required under axisymmetric conditions. With an initial void volume fraction, a localization bifurcation is possible under plane strain conditions while the matrix material is hardening. The value of the critical matrix hardening rate depends sensitively on the stress triaxiality. Even with an initial porosity, a localization bifurcation under axisymmetric conditions is effectively excluded for a workhardening matrix, $\bar{h} > 0$.

Yamamoto (1978) showed that an initial imperfection, in the form of a band with slightly increased porosity, could trigger localization in a porous solid under axisymmetric conditions. Figure 4.7, taken from Yamamoto (1978), shows critical strains to localization in a porous solid under both plane strain and axisymmetric conditions. As expected, based on the bifurcation analysis, localization occurs at much lower strains under plane strain conditions than under axisymmetric straining conditions. Also shown in Fig. 4.7 (b) is the band orientation in plane strain, where $\theta_0 = 0$ corresponds to a band orthogonal to the tensile axis. As the critical strain increases, i.e. for smaller imperfections, θ_0 decreases. The tendency for θ_0 to decrease with increasing localization strains also holds under axisymmetric conditions. A similar analysis has been used by Needleman and Triantafyllidis (1978) to study porosity induced local necking in thin sheets.

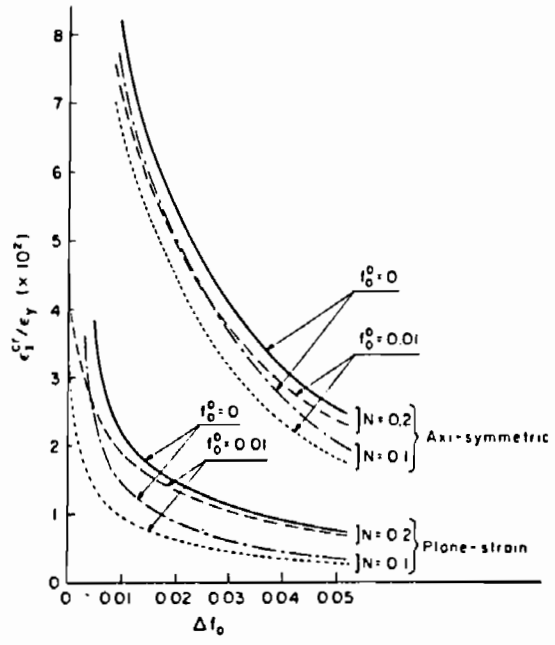

(a)

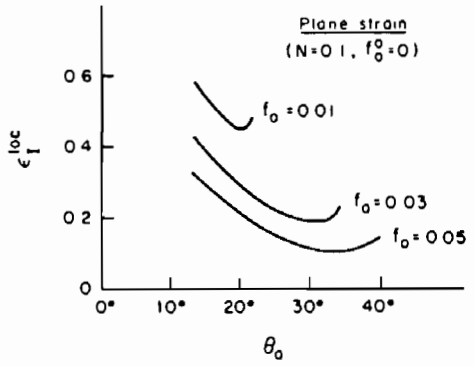

(b)

FIGURE 4.7. (a) Curves of critical strain for localization as a function of the initial void concentration in the band, f_0. (b) Curves of critical strain for localization versus initial band angle in plane strain. N is the hardening exponent of the matrix material (from Yamamoto, 1978).

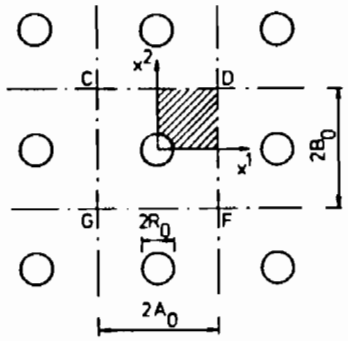

FIGURE 4.8. Doubly periodic array of circular cylindrical voids.

4.5 Void Interaction Effects

An early investigation in which interaction effects are rigorously accounted for is the numerical analysis of Needleman (1972) for an elastic-plastic solid containing a doubly periodic array of circular cylindrical voids, as shown in Fig. 4.8. Due to symmetries only the region hatched in Fig. 4.8 had to be analyzed, and finite strain effects were fully accounted for in the computations. Thus, final failure by necking of the ligaments to zero thickness could be approached in the numerical solutions, and linear extrapolations of the overall stress-strain curves were used to estimate the average strain at coalescence. The assumption of an array of parallel cylindrical voids is a strong idealization, but is very convenient computationally, since this allows for a planar analysis. It is expected that the results based on this idealization give quite a useful indication of actual void coalescence behavior.

A numerical finite element study by Andersson (1977) for voids in a rigid-perfectly plastic material has been continued to a stage very near final coalescence with neighboring voids. Here the focus was on voids just ahead of a moving crack tip, and therefore a state of uniaxial straining was assumed, so that the voids grew under high hydrostatic straining. These voids were taken to be initially spherical, and an axisymmetric model problem was solved, representing a periodic distribution of voids in the layer ahead of the crack tip. The analyses were used to estimate the total work of separation per unit area of new crack surface when crack growth occurs by a void coalescence mechanism. It was also found that in the uniaxial strain state analyzed the initially spherical voids grow into oblate spheroids rather than elongating in the main tensile direction.

An approximate representation of a material with a certain volume fraction of spherical voids can be obtained in terms of a spherical unit cell containing a concentric spherical void, where the loading or displacements on the outer surface is chosen in agreement with the overall stress or strain state of the material. This type of analysis accounts for the interaction between neighboring voids in a very approximate manner. Upper bound rigid-plastic analyses for such model problems have been used by Gurson (1975), to obtain the approximate overall yield condition for a void containing ductile material, as described in Section 4.3.

A detailed understanding of the effect of voids on the occurrence of material instabilities requires a micromechanical analysis that accounts for the nonuniform stress and strain fields around voids and the interaction between neighboring voids. Early studies of this type were carried out by McClintock, Kaplan and Berg (1966) and by Nagpal, McClintock, Berg and Subudhi (1972). Tvergaard (1981) carried out a full bifurcation analysis for the doubly periodic array of circular cylindrical voids previously analyzed by Needleman (1972). Here, the solution obtained by assuming symmetry conditions on all four edges of the region hatched in Fig. 4.8 represents the fundamental solution with a homogeneous macroscopic strain state, but taking full account of the nonuniform strain fields on the micro level around voids. The possibility of bifurcation into another periodic pattern was analyzed on the basis of Hill's (1958) general theory of uniqueness and bifurcation for elastic-plastic solids. In this bifurcation analysis several symmetry properties of the repetitive pattern were employed so that again only the hatched region in Fig. 4.8 had to be analyzed, and the analysis also incorporated the necessary conditions of equilibrium and compatibility on the shear band interface, which could only be satisfied on the average between the two different periodic deformation patterns. In Fig. 4.9 the first critical bifurcation points and the corresponding angles of inclination of the shear bands are marked on curves of nominal traction versus overall strain, for the model material subject to uniaxial plane strain tension. In predictions based on a continuum model bifurcation into a shear band mode is associated with loss of ellipticity of the governing differential equations, but in this full bifurcation analysis accounting for discrete voids the equations remain elliptic.

Bifurcation into a localized mode has also been studied for a periodic array of spherical voids (Tvergaard, 1982), based on an axisymmetric analysis for a circular cylindrical unit cell containing a spherical void. The outer surface of the unit cell had to remain cylindrical throughout the deformations, to approximately represent compatibility with neighboring cells, and a fixed ratio of the average true principal stresses was prescribed. This axisymmetric model cannot represent shear bands with arbitrary angle of inclination to the direction of tension, as was possible in the planar analysis (Tvergaard, 1981), but the special case of bands perpendicular to this direction was analyzed, as is mainly relevant under high triaxial tension.

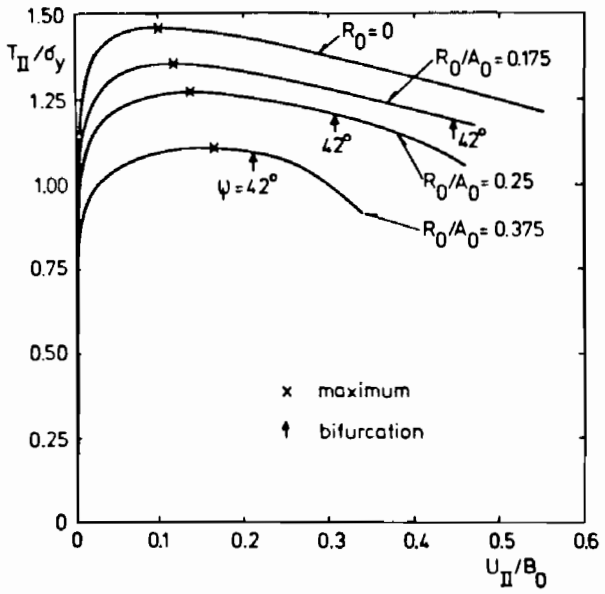

FIGURE 4.9. Nominal traction versus average strain for material containing a doubly periodic array of circular voids (from Tvergaard, 1981).

The analyses made use of the fact that during localization a slice of material undergoes deformation, while equilibrium and compatibility with the undeforming material outside this slice of material is retained. Based on a comparison of these bifurcation results with corresponding results using the material instability analysis described in Section 4.4, Tvergaard (1981, 1982) proposed modifying the yield condition (4.21) to

$$\Phi = \frac{\sigma_e^2}{\bar{\sigma}^2} + 2q_1 f \cosh\left(\frac{3q_2\sigma_h}{2\bar{\sigma}}\right) - 1 - q_3 f^2 = 0 \tag{4.40}$$

with

$$q_1 = 1.5 \qquad q_2 = 1 \qquad q_3 = q_1^2 = 2.25 \tag{4.41}$$

Analyses based on the same axisymmetric cell model problem have been carried out by Koplik and Needleman (1988) with the purpose of determining critical conditions for the onset of failure by coalescence of neighboring voids. These calculations show a shift from the state of axisymmetric elastic-plastic deformations to a mode of uniaxial straining where the plastic deformations localize to the ligament between neighboring voids. This localization is closely related to the bifurcations found by Tvergaard (1982). The two events would occur simultaneously if a longer cylindrical cell with two voids was analyzed, and earlier localization was also found by Koplik and Needleman (1988) in cases where a longer unit cell was considered.

Figure 4.10 shows results of these analyses for the values 1, 2 and 3 of the macroscopic stress triaxiality, $T = \Sigma_m/\Sigma_e$. Based on their cell model calculations, Koplik and Needleman (1988) suggested $q_1 = 1.25$ and $q_2 = 1$ in Eq. 4.40. It is seen in Fig. 4.10 that after the onset of localization the macroscopic effective strain E_e grows very little, while the macroscopic Mises stress Σ_e decays rapidly, and the rapid increase of the void volume fraction f marks the development of coalescence. It is also seen that the failure strain is significantly reduced for increasing stress triaxiality. In order to account for this rapid drop in stress carrying capacity, Tvergaard and Needleman (1984) suggested replacing f in Eq. 4.40 with the function $f^*(f)$, so that

$$\Phi = \frac{\sigma_e^2}{\bar{\sigma}^2} + 2q_1 f^* \cosh\left(\frac{3q_2\sigma_h}{2\bar{\sigma}}\right) - 1 - (q_1 f^*)^2 = 0 \tag{4.42}$$

where

$$f^* = \begin{cases} f & f \le f_c\ ; \\ f_c + \dfrac{f_u^* - f_c}{f_f - f_c}(f - f_c) & f \ge f_c \end{cases} \tag{4.43}$$

Here, f_f is the void volume fraction at which the stress carrying capacity vanishes, so that $f^*(f_f) = f_u^* = 1/q_1$.

The cell model studies in Koplik and Needleman (1988) and similar studies in Becker et al. (1988) suggested that f_c and f_f vary slowly with stress triaxiality and with matrix strain hardening, but depend strongly on the initial porosity. Figure 4.11, from Tvergaard (1990), shows the dependence of f_c on initial porosity according to these cell model studies. Figure 4.12 compares the overall stress strain behavior and void growth based on the modified Gurson constitutive relation with corresponding results based on Gurson's original yield function (Eq. 4.21) for the case with $T = 3$ in Fig. 4.5. The modified constitutive relation gives failure at realistic values of the void volume fraction.

The studies of void interaction effects discussed here are all based on simplifying assumptions that allow for planar analyses with cylindrical voids or axisymmetric analyses with spherical voids. More realistic models would generally require full three-dimensional numerical solutions, but such computations put very large requirements on computer time and storage. Full 3D computations have been carried out by Hom and McMeeking (1989) and Worswick and Pick (1990) for the growth of initially spherical voids in periodic cubic arrays. Very good agreement was found between the predictions of these full three dimensional analyses and corresponding predictions of axisymmetric cell models. The results of the 3D studies have been mainly used to evaluate the validity of approximations involved in various dilatant plasticity continuum models for porous materials. Tvergaard (1988) has analyzed 3D cubic arrays of larger voids in a matrix containing smaller voids. In this analysis the formation of the larger voids with approximately

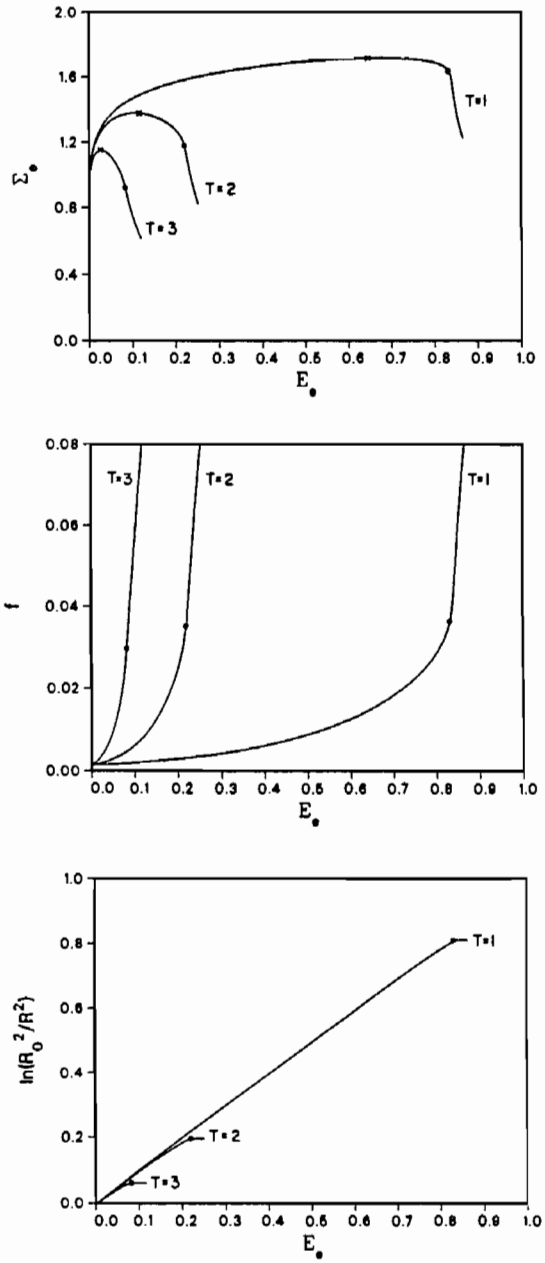

FIGURE 4.10. Finite element results for a cylindrical cell model with a spherical void and an initial void volume fraction $f_0 = 0.0013$, for different values of the stress triaxiality T (from Koplik and Needleman, 1988).

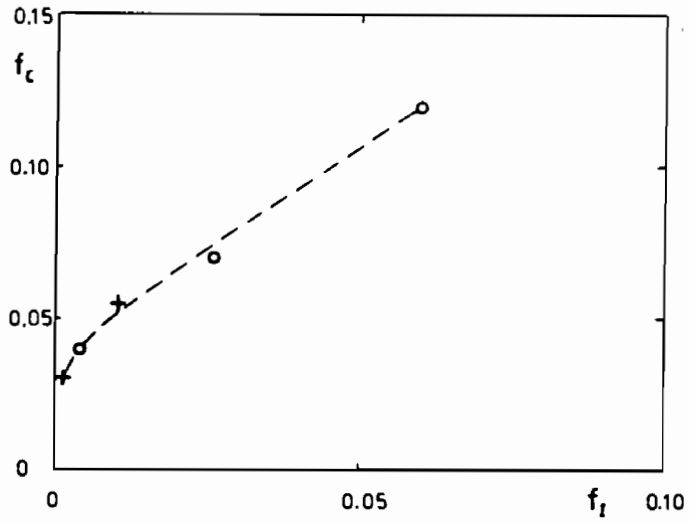

FIGURE 4.11. Dependence of the critical value f_c in Eq. 4.43 on the initial void volume fraction f_I according to various cell model studies (from Tvergaard, 1990).

spherical shape is formulated in terms of a porous ductile material model, and the focus is on the prediction of final fracture.

4.6 Boundary Value Problem Solutions

Calculations of localization and failure in a homogeneously deformed material element, provide much insight into the behavior of the constitutive relation. However, such calculations cannot capture a key feature that determines the observed ductile failure mode in test specimens and structural components; the redistribution of stress and deformation accompanying progressive micro-rupture. Here, some calculations that illustrate the development of failure modes in full specimens will be reviewed.

A characteristic feature of ductile fracture in structural metals is the contrast between the shear fracture mode observed in plane strain tensile specimens and the cup-cone mode observed in axisymmetric tensile specimens. In both cases, the deformations remain essentially homogeneous up to the maximum load point after which a diffuse neck develops. In the round bar tension test, diffuse necking is followed by a cup-cone type fracture, while typically in a plane strain tensile test of the same material, the deformation mode shifts to one involving localized shearing while the diffuse neck is rather shallow.

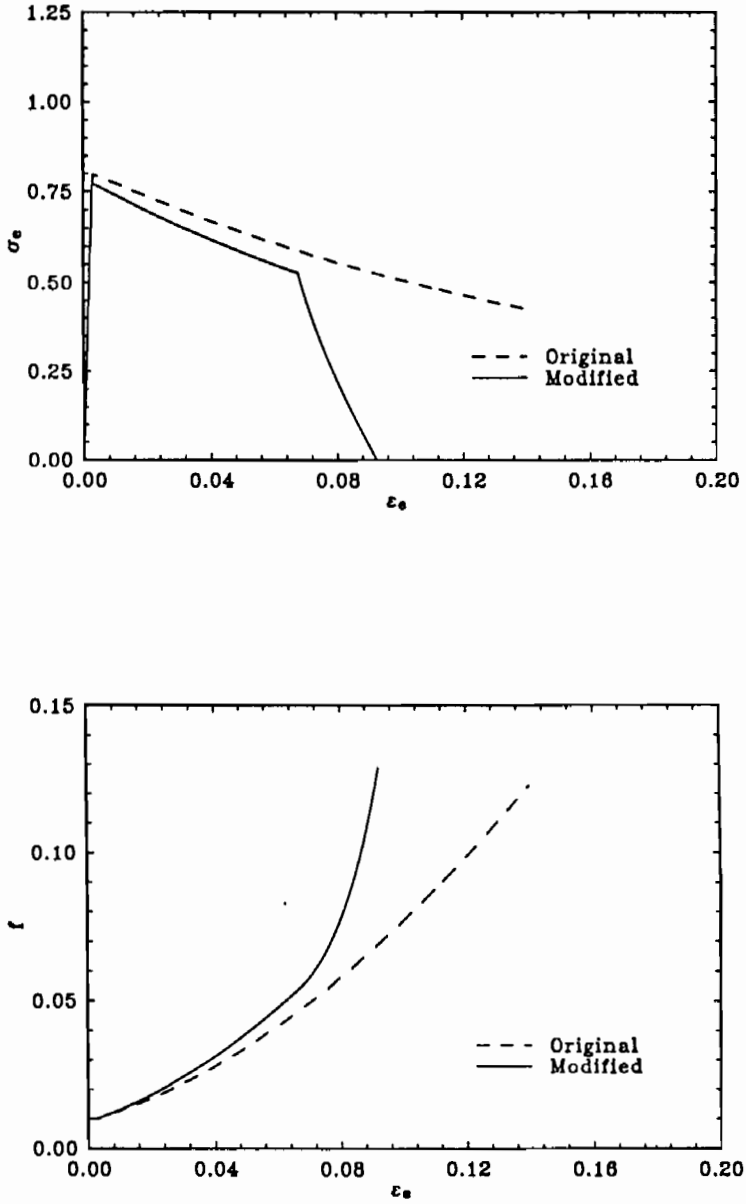

FIGURE 4.12. Comparison of overall stress strain behavior and void growth predictions based on the original, Eq. 4.21, and modified, Eq. 4.42, Gurson constitutive relations for a material element subject to uniaxial tension with a superposed hydrostatic tension, σ_h, with $T = \sigma_h/\sigma_e$. The matrix is ideally plastic and $f_0 = 0.002$.

Figures 4.13 and 4.14 show the fracture behaviors obtained from finite element calculations based on the modified Gurson constitutive relation, Eq. 4.42. In the calculations symmetry conditions are imposed so that only one quadrant of the specimen needs to be analyzed numerically and deformed finite element meshes are shown for this quadrant. Figure 4.13 is from Tvergaard and Needleman's (1984) finite element analysis of necking and failure in the tensile test, which incorporates a model for void nucleation into the formulation. The predicted fracture mode reproduces the essential features of a cup-cone fracture. Among the features typically observed in axisymmetric tensile tests of ductile metals is that voids initiate and grow in the center of the neck finally coalescing to form a central crack. There is a tendency for the crack to zig-zag, which is a consequence of shear localization being inhibited by the additional plastic work associated with the hoop strains that accompany shearing in the axisymmetric geometry. As the free surface is approached this axisymmetric constraint is relaxed, permitting the cone of the cup-cone fracture to form. This analysis shows how the interaction of the tendency to localization in a material weakened by void nucleation and growth together with a constraining geometrical effect lead to the cup-cone fracture. The development of failure has a significant effect on the overall load-displacement response of the specimen as shown in Fig. 4.13 (a). There is no corresponding geometrical constraint in plane strain tension so that, once initiated, a shear band can propagate across the entire specimen as illustrated in Fig. 4.14, which were obtained by Becker and Needleman (1986) using a rate dependent material model where Eq. 4.42 serves as a flow potential. In this case, the load drop is associated with the formation of the shear band and failure subsequently ensues as strain accumulates in the band.

These results illustrate the ability to qualitatively predict observed ductile failure behaviors. A meaningful quantitative comparison between predictions and experiment is more complex because of the path dependent and progressive nature of ductile fracture. Becker et al. (1988) have compared quantitative predictions of void growth, strength and ductility with detailed measurements in round notched bars. Various notch geometries were studied in order to obtain different stress histories. The tensile specimens were machined from partially consolidated and sintered iron powder compacts. The only experimentally determined quantities input into calculations in Becker et al. (1988) were the uniaxial stress-strain curve for the matrix material and the initial void volume fraction. The parameters q_1, q_2, f_c and f_f entering the porous plastic constitutive description were chosen to provide a reasonable fit of both strength and void growth predictions with results of micro-mechanical models of periodic arrays of voids as discussed in Section 4.5.

Figure 4.15 (a) shows a finite element mesh illustrating the axisymmetric specimen geometry and predicted evolution of the minimum section area,

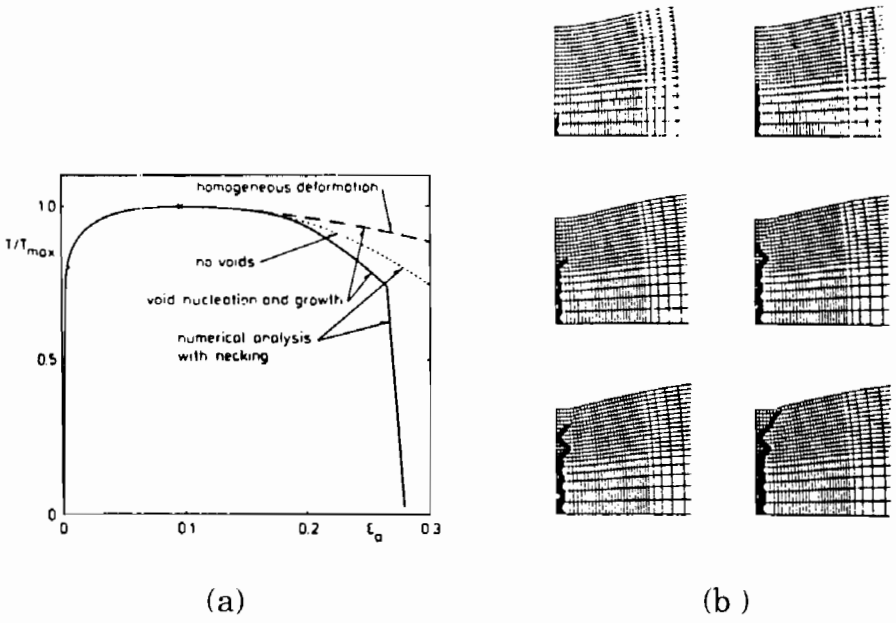

FIGURE 4.13. (a) Curves of load versus imposed strain and (b) crack growth in the neck for axisymmetric tension. In (b), triangular elements that have undergone a complete loss of stress carrying capacity are painted black (from Tvergaard and Needleman, 1984).

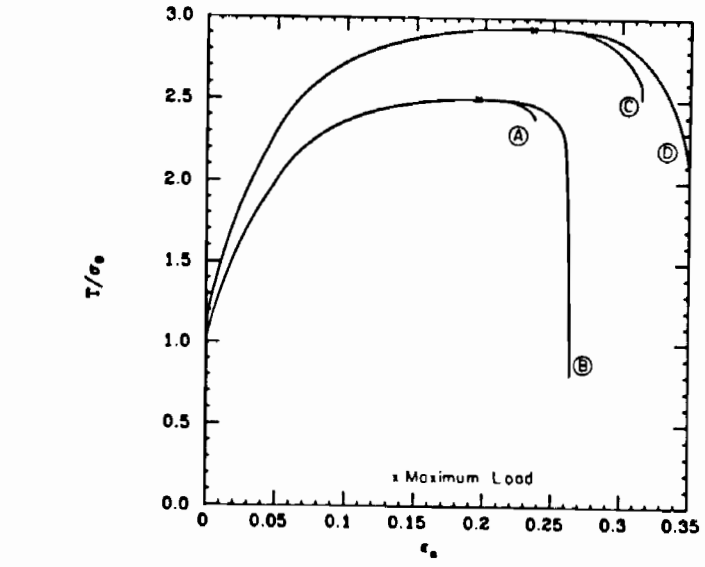

(a)

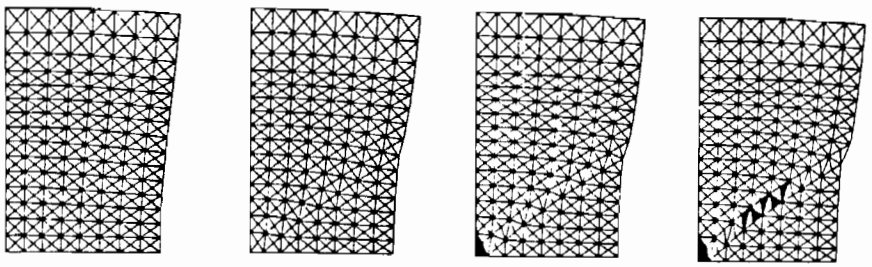

(b)

FIGURE 4.14. (a) Curves of load versus imposed strain and (b) crack growth in the neck for plane strain tension. The curve marked B in (a) pertain to the deformed meshes shown in (b), where triangular elements that have undergone a complete loss of stress carrying capacity are painted black (from Becker and Needleman, 1986).

$\ln(R_0^2/R^2)$, and the void volume fractions, f, measured at the center of the specimens. Also shown in Figs. 4.15 (b) and 4.15 (c) are measurements for eight specimens with 7% initial void volume fraction and one specimen with a 1% initial void fraction. The predictions are quite good at lower strains but the model somewhat under predicts void growth at large strains. Similar good agreement was found in comparisons made between prediction and experiment for other notch geometries.

4.7 Additional Considerations

When voids deform in a material subject to low triaxial tension the void volume grows little or the voids may even collapse into shapes like cracks or needles, as has been found by Budiansky, et al. (1982) for isolated voids. Often voids nucleate from a particle by debonding of the particle-matrix interface, and in such circumstances contact between the particle and the void surface may have a significant effect on void growth (Fleck, Hutchinson and Tvergaard, 1989). Figure 4.16 shows curves of normalized void dilatation rates versus stress triaxiality for an isolated void that has nucleated from a rigid spherical inclusion, in an elastic-perfectly plastic material subject to an axisymmetric stress state. At values of the triaxiality parameter around zero it is seen that the interaction with the particle enforces a void volume increase, because the contact with the particle gives rise to an internal pressure on the void surface in the transverse direction. For triaxialities higher than about 0.6 the presence of a particle inside the void has no influence, as the void expands in all directions.

Contact between particle and void surface is an important effect in simple shear, where an unfettered void closes as it deforms. This has been studied by Fleck et al. (1989) in terms of a planar elastic-perfectly plastic analysis for a row of voids in a shear field, with the geometry (Fig. 4.17) chosen to model experiments of Cowie, Azrin and Olson (1987). The development of the average shear stress, Σ_{12}, and the cross-sectional void area, A_v versus shear strain, γ, are shown in Fig. 4.18 for a superposed tensile or compressive stress, Σ_{22}. It is seen that for negative Σ_{22} the void volume still increases in the presence of a particle, but decays when there is no particle. The same type of behavior has been found for pure shear, $\Sigma_{22} = 0$.

When the stress triaxiality is high, material elasticity can have a major effect on the course of void evolution, even though the elastic strains remain small. This is because of the existence of a cavitation instability driven by the elastic energy in the surrounding material. For an isolated void in an elastic-plastic solid subject to remote hydrostatic tension there is a critical stress at which the void growth rate becomes unbounded, Bishop, Hill and Mott (1945), Hill (1950). This instability does not occur for a rigid-plastic solid. There has been much recent interest in cavitation instability

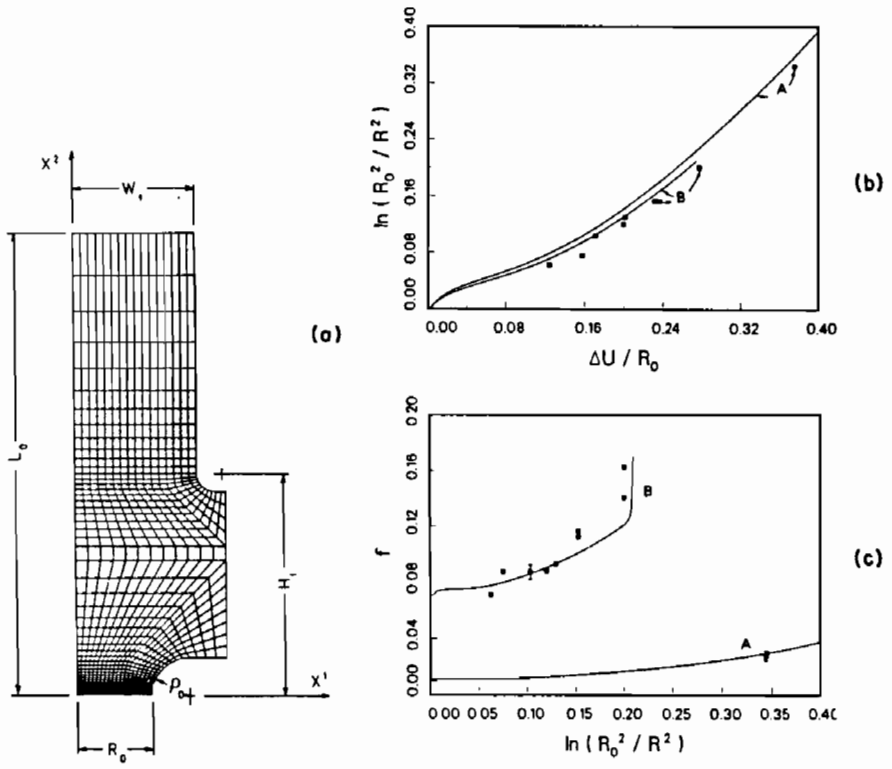

FIGURE 4.15. (a) Specimen geometry and finite element mesh. (b) and (c) respectively show the experimental and calculated development of the minimum section and porosity evolution as a function of strain for 1% and 7% initially porous notched bars from (Becker et al., 1988).

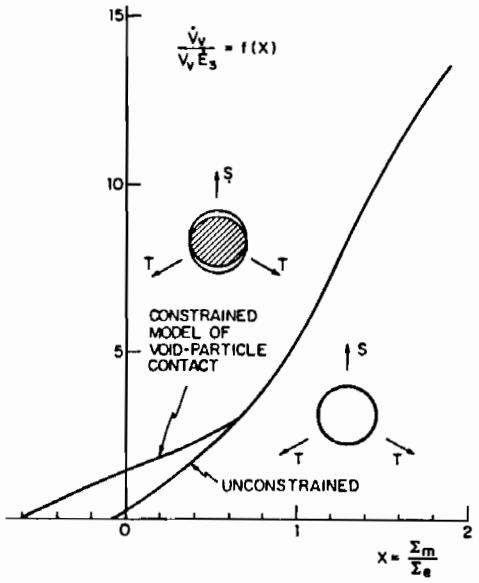

FIGURE 4.16. Normalized dilation rate following nucleation as a function of stress triaxiality (from Fleck et al., 1989).

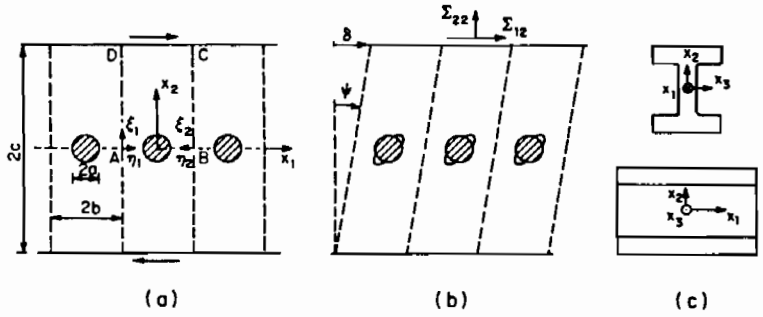

FIGURE 4.17. Model for the nucleation and growth of 2D voids in simple shear. (a) Starting geometry. (b) Subsequent to nucleation. (c) Test specimen modelled (from Fleck et al., 1989).

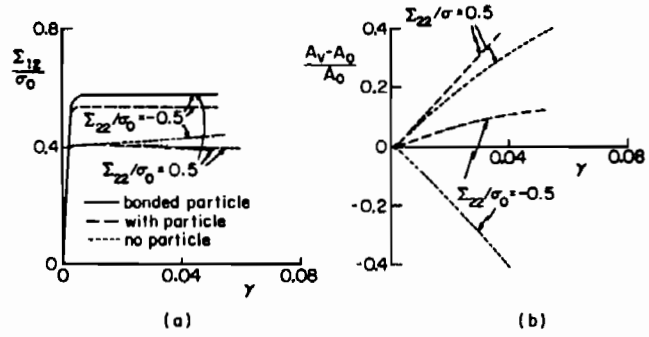

FIGURE 4.18. Effect of a superposed normal stress, Σ_{22}, for $a/b = 0.25$ in Fig. 4.17 (from Fleck et al., 1989).

phenomena from a variety of perspectives, e.g. Ball (1982), Horgan and Abeyaratne (1986), Abeyaratne and Hou (1989). Here, we illustrate the phenomenon by outlining the classic analysis for an isolated void in an isotropic, incompressible elastic-plastic solid subject to remote hydrostatic tension. The development and notation follows that in Huang et al. (1991).

We define R as the distance, in the current state, of a material point from the void center, R_i is the initial void radius and R_0 is the current void radius.

Equilibrium is expressed by

$$\frac{d\sigma_r}{dR} + \frac{2(\sigma_r - \sigma_\theta)}{R} = 0 \tag{4.44}$$

and incompressibility implies

$$\epsilon_r = -2\epsilon_\theta = \frac{2}{3}\ln[1 - (R_0^3 - R_i^3)/R^3] \tag{4.45}$$

The stress-strain relation for a Mises solid is of the form

$$\frac{\bar{\sigma}}{\sigma_y} = f(\bar{\epsilon}) \tag{4.46}$$

where

$$\bar{\sigma} = |\sigma_r - \sigma_\theta| \qquad \bar{\epsilon} = |\epsilon_r| \tag{4.47}$$

The boundary conditions are

$$\sigma_r(R_0) = 0 \qquad \sigma_r(\infty) = \sigma_\infty \tag{4.48}$$

From equilibrium and incompressibility,

$$\frac{\sigma_\infty}{\sigma_y} = -2\int_1^\infty f\left[\frac{2}{3}\ln\left[1 - \frac{(1 - (R_i/R_0)^3}{x^3}\right]\right]\frac{dx}{x} \tag{4.49}$$

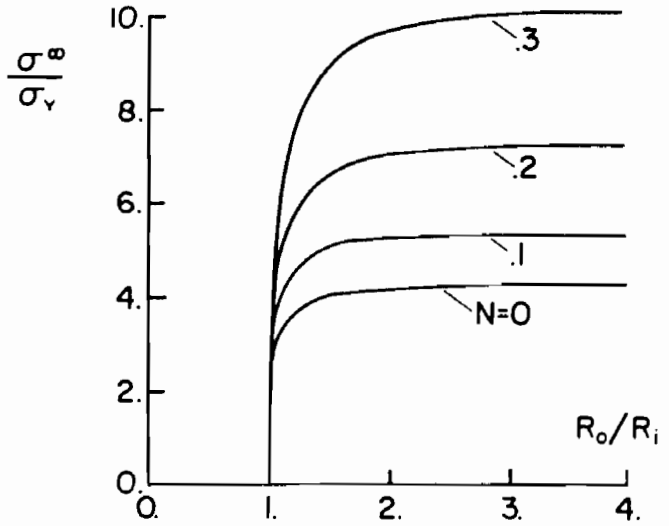

FIGURE 4.19. Remote stress versus radius of the cavity for hardening and non-hardening solids under spherically symmetric loading (from Huang et al., 1991).

The cavitation limit, $\sigma_\infty \to S$, is reached when $R_0/R_i \to \infty$. From Eq. 4.49,

$$\frac{S}{\sigma_y} = -2\int_1^\infty f\left[\frac{2}{3}\ln[1-x^{-3}]\right]\frac{dx}{x} \tag{4.50}$$

For a perfectly plastic solid, Eq 4.50 gives the result, Hill (1950),

$$\frac{S}{\sigma_y} \approx \frac{2}{3}\left[1+\ln(\frac{2}{3\epsilon_y})\right] \tag{4.51}$$

Figure 4.19, from Huang et al. (1991), shows curves of remote stress versus cavity radius for a power law solid, $\bar{\sigma} \propto \bar{\epsilon}^N$. Because of the cavitation limit, the void growth rate at high stress triaxiality can be significantly greater than predicted based on a rigid-plastic analysis, as shown in Fig. 4.20.

Micromechanical analyses of porous solids have generally presumed that the voids are distributed in some regular pattern. However, void distribution effects have been shown to play a significant role in limiting ductility, both experimentally, Dubensky and Koss (1987), and theoretically, Becker (1987). Becker (1987) analyzed void growth and coalescence in a small material element, with the material characterized by the modified Gurson (1975) constitutive relation, but with a nonuniform initial distribution of the void volume fraction. Becker (1987) found a significantly smaller fracture strain for a solid with a non-uniform porosity distribution than for a solid with a uniform porosity at the average value. There was a negligible

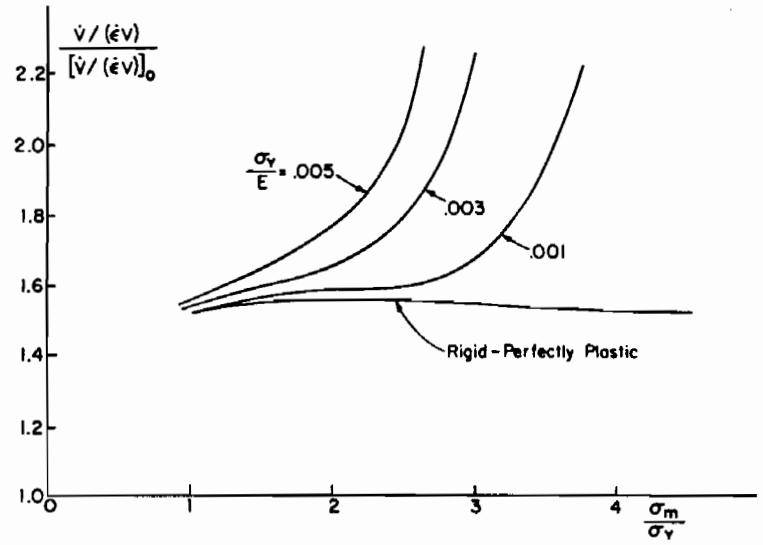

FIGURE 4.20. Effect of elasticity on the dilation rate of nominally spherical voids. The volumetric growth rate is normalized by that obtained from Eq. 4.14 using $(\dot{V}/\dot{\epsilon}_0 V)_0 = 3\dot{R}_0/\dot{\epsilon}_0 R_0$ (from Huang et al., 1991).

effect of the nonuniformity prior to the localization that precedes fracture. The quantification of distribution effects on ductile fracture processes remains a challenge for future research.

The phenomenological yield surfaces that have been proposed for porous plastic solids have all been smooth. Because of the non-homogeneous stress state around a void, a change in loading direction can result in unloading of part of the current plastic zone. This leads to a vertex on the yield surface as illustrated in Mear (1990). The vertices found by Mear (1990) were "blunt" so that the response did not differ greatly from what would be predicted based on a smooth yield surface.

Acknowledgments: A.N. is grateful for the support provided by the Brown University Materials Research Group on the Micromechanics of Failure-Resistant Materials, funded by the National Science Foundation. The work of JWH was supported in part by the Materials Research Laboratory (Grant NSF-DMR-89-20490) and the Division of Applied Sciences.

REFERENCES

Abeyaratne, R. and Hou, H.-S. (1989). Growth of an infinitesimal cavity in a rate dependent solid. *J. Appl. Mech.*, 56:40.

Andersson, H. (1977). Analysis of a model for void growth and coalescence ahead of a moving crack tip. *J. Mech. Phys. Solids*, 25:217.

Ball, J. M. (1982). Discontinuous equilibrium solutions and cavitation in nonlinear elasticity. *Phil Trans. R. Soc. London*, A306:557.

Bishop, R. F. and Hill, R. (1951). A theory of the plastic distortion of a polycrystalline aggregate under combined stresses. *Phil. Mag. Ser. 7*, 42:414.

Bishop, R. F., Hill, R. and Mott, N. F. (1945). The theory of indentation and hardness tests. *Proc. Phys. Soc.*, 57:147.

Beachem, C. D. (1963). An electron fractographic study of the influence of plastic strain conditions upon ductile rupture processes in metals. *Trans. ASM* 56:318.

Becker, R. (1987). The effect of porosity distribution on failure. *J. Mech. Phys. Solids*, 35:577.

Becker, R. and Needleman, A. (1986). Effect of yield surface curvature on necking and failure in porous plastic solids. *J. Appl. Mech.*, 53:491.

Becker, R., Needleman A., Richmond, O., and Tvergaard, V. (1988). Void growth and failure in notched bars. *J. Mech. Phys. Solids*, 36:317.

Berg, C. A. (1962). The motion of cracks in plane viscous deformation. In Rosenberg, R. M., editor, *Proc. Fourth U.S. National Congress of Applied Mechanics*, ASME, NY, 2:885.

Budiansky, B., Hutchinson, J. W. and Slutsky, S. (1982). Void growth and collapse in viscous solids. In H. G. Hokins and M. J. Sewell, editors, *Mechanics of Solids*, Pergamon Press, Oxford, 13.

Cowie, J. G., Azrin, M. A. and Olson, G. B. (1990). Micro-void formation during shear deformation of ultrahigh strength steels. In Olson, G. B. et al., editors, *Innovations in Ultrahigh-Strength Steel Technology, Proceedings of the 34th Sagamore Army Materials Research Conference*, U.S. Government Publication, 357.

Dubensky, E. M. and Koss, D. A. (1987). Void/pore distributions and ductile fracture. *Met. Trans.*, 18A:1887.

Fleck, N. A., Hutchinson, J. W. and Tvergaard, V. (1989). Softening by void nucleation and growth in tension and shear. *J. Mech. Phys. Solids*, 37:515.

Fleck, N. A., Otoyo, H. and Needleman, A. (1991). Indentation of porous solids. *Int. J. Solids Struct*, in press.

Gilormini, P., Licht, C. and Suquet, P. (1988). Growth of voids in a ductile matrix: a review. *Arch. Mech.* 40:43.

Guennouni, T. and Francois, D. (1987). Constitutive equations for rigid plastic or viscoplastic materials containing voids. *Fatigue Fract. Engng. Mater. Struct.*, 10:399.

Gurland, J. and Plateau, J. (1963). The mechanism of ductile rupture of metals containing inclusions. *Trans. ASM*, 56:442.

Gurson, A. L. (1975). *Plastic Flow and Fracture Behavior of Ductile Materials Incorporating Void Nucleation, Growth and Interaction.* Ph.D. Thesis, Brown University.

Hadamard, J. (1903). *Leçons sur la Propagation des Ondes et les Équations de L'Hydrodynamique*, Paris, Chp. 6.

Hancock, J. W. and Brown, D. K., (1983). On the role of strain and stress state in ductile failure. *J. Mech. Phys. Solids*, 31:1.

Hancock, J. W. and MacKenzie, A. C. (1976). On the mechanisms of ductile failure in high-strength steels subjected to multi-axial stress-states. *J. Mech. Phys. Solids*, 24:147.

Hill, R. (1950). *The Mathematical Theory of Plasticity*, Clarendon Press, Oxford.

Hill, R. (1958). A general theory of uniqueness and stability in elastic-plastic solids. *J. Mech. Phys. Solids*, 6:236.

Hill, R. (1962). Acceleration waves in solids. *J. Mech. Phys. Solids*, 10:1.

Hom, C. L. and McMeeking, R. M. (1989) Void growth in elastic-plastic materials. *J. Appl. Mech.*, 56:309.

Horgan, C. O. and Abeyaratne, R. (1986). A bifurcation problem for a compressible nonlinearly elastic medium: growth of a microvoid. *J. Elast.*, 16:189.

Huang, Y. (1989) Accurate dilation rates for spherical voids in triaxial stress fields. Report Mech-155. Division of Applied Sciences. Harvard University.

Huang, Y., Hutchinson, J. W. and Tvergaard, V. (1991). Cavitation instabilities in elastic-plastic solids. *J. Mech. Phys. Solids*, 39:223.

Koplik, J., and Needleman, A. (1988). Void growth and coalescence in porous plastic solids. *Int. J. Solids Struct.*, 24:835.

Lemaitre, J. (1985). A continuous damage mechanics model for ductile fracture. *J. Engng. Mat. Tech.*, 107:83.

Mandel, J. (1966). Conditions de stabilité et postulat de Drucker. In Kravtchenko, J. and Sirieys, P. M., editors, *Rheology and Soil Mechanics*, Springer-Verlag, 58.

Marini, B., Mudry, F. and Pineau, A. (1985). Ductile rupture of A508 steel under nonradial loading. *Engng. Fract. Mech.*, 22:375.

Mear, M. E. (1990). On the plastic yielding of porous metals. *Mech. Matl.* 9:33.

McClintock, F. A. (1968). A criterion for ductile fracture by the growth of holes. *J. Appl. Mech.*, 35:363.

McClintock, F. A., Kaplan, S. M. and Berg, C. A. (1966). *Int. J. Frac. Mech.*, 2:614.

Nagpal, V., McClintock, F. A., Berg, C. A. and Subudhi, M. (1972). Traction-displacement boundary conditions for plastic fracture by hole growth. In Sawczuk, A., editor, *Foundations of Plasticity*, Noordhoff, 365.

Needleman, A. (1972). Void growth in an elastic-plastic medium. *J. Appl. Mech.*, 39:964.

Needleman, A. and Rice J. R., (1978). Limits to ductility set by plastic flow localization. In Koistinen, D. P. and Wang, N. M., editors, *Mechanics of Sheet Metal Forming*, Plenum Press, New York, 237.

Needleman, A. and Triantafyllidis, N. (1978). Void growth and local necking in biaxially stretched sheets. *J. Engng. Mat. Tech.*, 10:164.

Puttick, K. E. (1959). Ductile fracture in metals. *Phil. Mag.*, 4:964.

Rice, J. R. (1977). The localization of plastic deformation. In Koiter, W. T., editor, *Theoretical and Applied Mechanics*, North-Holland, 207.

Rice, J. R. and Tracey, D. M. (1969). On the ductile enlargement of voids in triaxial stress fields. *J. Mech. Phys. Solids*, 17:201.

Rogers, H. C. (1960). The tensile fracture of ductile metals. *Trans. Metall. Society AIME*, 218:498.

Shima, S. and Oyane, M. (1976). Plasticity theory for porous metals. *Int. J. Mech. Sci.*, 18:285.

Tipper, C. F. (1949). The fracture of metals. *Metallurgia*, 33:133.

Tvergaard, V. (1981). Influence of voids on shear band instabilities under plane strain conditions. *Int. J. Fract.*, 17:389.

Tvergaard, V. (1982). On localization in ductile materials containing spherical voids. *Int. J. Fract.*, 18:237.

Tvergaard, V. (1988). 3D-analysis of localization failure in a ductile material containing two size-scales of spherical particles. *Engng. Fract. Mech.*, 31:421.

Tvergaard, V. (1990). Material failure by void growth to coalescence. Adv. Appl. Mech., 27:83.

Tvergaard, V. and Needleman, A. (1984). Analysis of cup-cone fracture in a round tensile bar. *Acta Metall.*, 32:157.

Worswick, M. J. and Pick, P. J. (1990). Void growth and constitutive softening in a periodically voided solid. *J. Mech. Phys. Solids* 38:601.

Yamamoto, H. (1978). Conditions for shear localization in the ductile fracture of void-containing materials. *Int. J. Fract.*, 14:347.